HHS Public Access

Author manuscript

ACS Appl Bio Mater. Author manuscript; available in PMC 2020 March 18.

Published in final edited form as:

ACS Appl Bio Mater. 2019 March 18; 2(3): 1141–1147. doi:10.1021/acsabm.8b00755.

Electrospray Functionalization of Titanium Dioxide Nanoparticles with Transferrin for Cerenkov Radiation Induced Cancer Therapy

Nathan A. Reed[†], **Ramesh Raliya**[†], **Rui Tang**[‡], **Baogang Xu**[‡], **Matthew Mixdorf**[‡], **Samuel Achilefu**[‡,§,‖], and **Pratim Biswas**[*,†]

[†]Aerosol and Air Quality Research Laboratory, Department of Energy, Environmental and Chemical Engineering, Washington University in St. Louis, St. Louis, Missouri 63130, United States

[‡]Optical Radiology Lab, Mallinckrodt Institute of Radiology, Department of Radiology, Washington University School of Medicine, St. Louis, Missouri 63130, United States

[§]Department of Biomedical Engineering, Washington University in St. Louis, St. Louis, Missouri 63130, United States

[‖]Department of Biochemistry and Molecular Biophysics, School of Medicine, Washington University in St. Louis, St. Louis, Missouri 63130, United States

Abstract

Titanium dioxide (TiO_2) nanoparticles have shown success as photosensitizers in the form of light-based cancer therapy called Cerenkov radiation induced therapy (CRIT). While TiO_2 nanoparticles have been reported to be an effective therapeutic agent, there has been little work to control their functionalization and stability in aqueous suspension. In this work, the controlled coating of 25 nm diameter TiO_2 nanoparticles with the glycoprotein transferrin (Tf) for application in CRIT was demonstrated using an electrospray system. Monodisperse nanoscale droplets containing TiO_2 and Tf were dried during flight, coating the proteins on the surface of the metal oxide nanoparticles. Real-time scanning mobility particle sizing, dynamic light scattering, and transmission electron microscopy show efficient control of the Tf coating thickness when varying the droplet size and the ratio of Tf to TiO_2 in the electrospray precursor suspension. Further, the functionality of Tf-coated TiO_2 nanoparticles was demonstrated, and these particles were found to have enhanced targeting activity of Tf to the Tf receptor after electrospray processing. The electrospray-coated Tf/TiO_2 particles were also found to be more effective at killing the multiple myeloma cell line MM1.S than that of nanoparticles prepared by other reported functionalization methods. In summary, this investigation not only provides a single-step functionalization technique for

[*]*Corresponding Author* Pratim Biswas: pbiswas@wustl.edu. Tel.: +1-314-935-5548. Fax: +1-314-935-5464.

Author Contributions

The manuscript was written through contributions of all authors. NR, RR, SA, and PB designed the study. RR and NR performed material synthesis and characterization. NR completed coating experiments. BX and RT did binding affinity studies. MM and RT performed cell culturing and *in vitro* cell viability assays. PB and SA provided supervision of the project. All authors have given approval to the final version of the manuscript.

Notes

The authors declare no competing financial interest.

nanomaterials used in Cerenkov radiation induced therapy but also elucidates an electrospray coating technique for nanomaterials that can be used for a wide range of drug design and delivery purposes.

Graphical Abstract

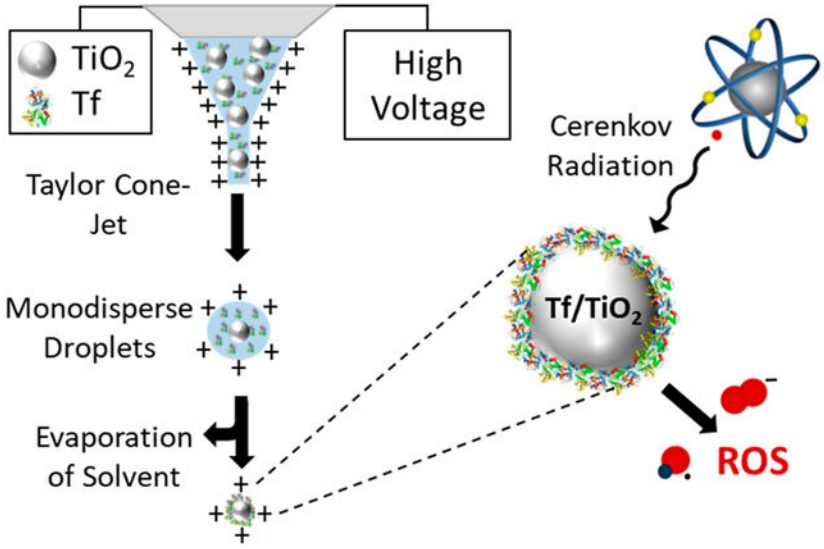

Keywords

electrospray; titanium dioxide; transferrin; functionalization; multiple myeloma; Cerenkov radiation induced therapy

INTRODUCTION

Multiple myeloma (MM) is a hematological cancer caused by malignant plasma cells within bone marrow. In the United States, MM is the second most common hematologic cancer, accounting for 1% of all cancer deaths. While the occurrence of MM is relatively low compared to many other cancers, the 5-year survival rate is below 40%.[1] Many patients respond well to treatment from several forms of chemotherapy, which often lead to periods of remission. However, remission induced by even the most effective current chemotherapies is short-lived, and patients ultimately relapse and die from disease progression. Although the mechanisms of the cancer's growth and its resistance to conventional therapies are being elucidated, it is clear that new therapeutic approaches are needed to increase treatment efficacy and reduce relapse. Recently, nanomaterials including functionalized metal, metal oxide, micelles, and liposomes have been explored as novel therapies and as materials to enhance current therapies.[2-10] Among these new materials, metal oxide photosensitizer nanoparticles have shown significant promise in light-based cancer therapy, but there are still significant scientific gaps in their functionalization, stability, and optimization for therapy. In this work, we present an electrospray method of functionalizing TiO_2 nanoparticles for the treatment of multiple myeloma and other forms of cancer.

Electrospray systems, when operated in the Taylor cone-jet regime, have been broadly utilized to produce monodisperse ionized droplets in a wide size range. While the technique is most commonly used to produce macromolecular ions for mass spectrometry, it has also been studied for generating monodisperse droplets for the synthesis and self-assembly of nanomaterials.[11, 12] Recently, electrospray has been used to generate nanoparticle standards,[13] fabricate solar cells,[12, 14] and deliver nanoparticles noninvasively to the brain of locusts.[15] Electrospray has also been extended to the synthesis of polymer and protein nanoparticles for biomedical applications.[16-20] Many of these studies incorporate drug molecules into the electrospray synthesized nanoparticles to create biocompatible drug carriers.[21] In this paper, the use of an electrospray system to efficiently coat the protein transferrin (Tf) on the surface of titanium dioxide (TiO_2) nanoparticles in a single step is demonstrated. These functionalized nanoparticles are used for a light-based cancer therapy, known as Cerenkov radiation induced therapy (CRIT). CRIT takes advantage of cancer cells' inherent susceptibility to reactive oxygen species (ROS) by spatiotemporally controlling the generation of cytotoxic ROS by exposing nanophotosensitizers, such as TiO_2, to ultraviolet (UV) light. Other forms of light-based cancer therapy traditionally have limited application beyond superficial or endoscopically accessible tissues due to the shallow penetration of light in tissue, especially for shorter wavelengths. To circumvent the limited penetration of UV light, positron emission tomography (PET) radiopharmaceuticals are used as a source of UV light. As they circulate throughout the body, these compounds emit UV light called Cerenkov radiation (CR), which occurs when positrons emitted from the radionuclide travel faster than the speed of light within the body. TiO_2 nanoparticles absorb this UV light and become excited, generating an electron and hole pair on the surface of the nanoparticle. This electron and hole react with water and oxygen to generate cytotoxic hydroxyl and superoxide radicals *in vivo*.[3,22] To target these nanoparticles to cancer cells, Tf, a blood plasma glycoprotein that transports iron throughout the body, is coated on their surface and functions as a ligand for Tf receptors, which many cancer cells overexpress.[23,24] By coating Tf on the surface of TiO_2 we can first target cancer cells and then separately expose them to radionuclide-induced CR. The result is CRIT confined to the cancer cell microenvironment, thus avoiding off-target toxicity.[3]

TiO_2 is extensively used as a photocatalyst due to its efficient absorption of UV light resulting in the generation of radicals including hydroxide and superoxide in the presence of water and oxygen.[25-28] Previous work has shown that anatase TiO_2 nanoparticles have the highest photocatalytic activity of any stable phase.[29] Jiang et al. also observed that, among a wide range of tested particles sizes, the highest ROS activity per unit area was observed for particles with an average diameter of 30 nm. ROS production from our particles follows a similar trend, showing anatase TiO_2 nanoparticles with an average diameter of 25 nm producing the highest ROS activity per unit area. In this work we focus on 25 nm anatase TiO_2 nanoparticles, although 5, 10, 15, and 50 nm nanoparticles were also successfully coated with Tf using electrospray.

In previous work on CRIT using Tf-coated TiO_2, the authors functionalized the nanoparticles by mixing Tf and TiO_2 in a suspension and sonicating for several minutes. While this functionalization method was successful, a significant amount of unbound Tf was observed in the suspension; an unspecified amount of final product was lost in filtering; and

there was little control of the Tf coating thickness on the surface of the TiO_2.[3] In this work we utilize electrospray to controllably coat Tf on the surface of TiO_2 nanoparticles by drying monodisperse droplets containing varying concentrations of Tf and controlled concentrations of TiO_2 nanoparticles. During electrospray processing, once a stable Taylor Cone jet forms, monodisperse droplets are emitted from the end of the capillary. These droplets move with the CO_2 sheath flow and immediately begin to dry. During drying, the Tf and TiO_2 nanoparticles in the charged droplets move closer and closer together, eventually confining Tf to the TiO_2 nanoparticle surface when the droplet fully dries, forming charged Tf/TiO_2 nanoparticles.

The Tf/TiO_2 nanoparticles were characterized in real time using a scanning mobility particle sizer and offline using transmission electron microscopy and dynamic light scattering. During our electrospray processing, the droplets were exposed to a large electric field and low pH. To test the effect of electrospray processing on the targeting of our Tf/TiO_2 nanoparticles, we used microscale thermophoresis to measure the binding affinity of fluorescently tagged Tf to the Tf receptor. To further validate the efficiency of our nanoparticles and coating process, an *in vitro* CRIT study was performed on an MM1.S cancer cell line. These cells are from a human multiple myeloma (MM) cell line and represent an *in vitro* model for multiple myeloma.[30]

RESULTS AND DISCUSSION

Titanium dioxide (TiO_2) nanoparticles were synthesized by hydrolysis of TTIP under a controlled temperature, pH, and ratio of TTIP to water and ethanol. The TEM micrograph in Figure 1 shows the successful synthesis of TiO_2 nanoparticles with an average diameter of 25 nm (±3.2 nm). XRD analysis of these nanoparticles, shown in Figure 2, indicates they are anatase TiO_2. DLS measurements, found in Table 1, further describe their size in water at pH 4 and show the hydrodynamic number mean diameter of these bare TiO_2 nanoparticles as 25.4 nm with a polydispersity index of 0.38.

When preparing precursor suspensions, it is critical to ensure the TiO_2 nanoparticles and Tf are as stable as possible so that aggregation does not occur in the capillary. For efficient and tightly controlled electrospray coating of Tf on TiO_2, it is ideal to only have one TiO_2 nanoparticle and many Tf molecules per droplet. This was achieved by changing the conductivity, zeta potential, flow rate, and precursor concentration of the sprayed suspension. The isoelectric points of all precursor Tf and TiO_2 nanoparticle suspensions were found to be very similar, between pH of 6.5 and 7.5 (Figure 3). Due to the relatively low stability of these suspensions in ultrapure water, the pH was lowered to approximately 4 using nitric acid, which increased the zeta potential to 35–40 mV, significantly increasing their stability in suspension. Nitric acid had the dual purpose of increasing the conductivity of the nanoparticle suspension to 0.3 S/m for electrospray processing. While pH was important for stability, the conductivity of the suspension was more critical and was more tightly controlled than pH. Using a dilute precursor suspension further helped assure that only single TiO_2 nanoparticles were in each droplet, but too much dilution also increased the number of empty droplets and those containing only Tf. By balancing these factors and droplet size, an ideal concentration was determined to be 1 mg/mL of TiO_2 nanoparticles.

Controlled functionalization of TiO_2 nanoparticles with Tf was successfully demonstrated by adjusting the concentration of Tf in the precursor suspension from 0 to 25 μM with a constant 1 mg/mL concentration of TiO_2 nanoparticles. The thickness of the Tf coating was estimated assuming the Tf's were noncoalescing spheres with a diameter of 6.6 nm.[31-33] The SMPS measurements shown in Figure 4 highlight the close match between the geometric mean diameter (GMD) of nanoparticles and the expected Tf/TiO_2 nanoparticle size for each Tf concentration. Further experiments were completed with Tf only at the same concentrations. The SMPS data shown in Figure 5 further validate that the measured GMD of Tf nanoparticles formed from dried electrospray drops match the expected size. The TEM images in Figure 6 show TiO_2 nanoparticles with a coating on their surface that closely correlates with the expected Tf coating thickness. The DLS data in Table 1 show similar number mean diameters as those measured by SMPS and TEM for each concentration of Tf. While the PDI for these nanoparticles is relatively high, they are very similar for all samples including the bare TiO_2 nanoparticles.

Once Tf was successfully coated on the surface of TiO_2 nanoparticles the next step was to determine the effect of electrospray processing on Tf's affinity to bind to the Tf receptor. This binding was measured by microscale thermophoresis (MST), a technique for the study of biomolecular interactions in an aqueous environment, which does not require immobilization of either reaction partner.[34] MST exploits the directed movement of molecules along a microscopic temperature gradient. The rate and direction of movement are dependent upon the size, charge, and solvation shell of the species under study. Any changes in this environment have the potential to change the thermophoretic movement of the species.[35] This technique can distinguish very small changes to protein surfaces that occur, for example, when a small molecule binds to the surface of a large fluorescently labeled protein,[36-38] in our case, the fluorescent protein coated nanoparticle. MST analysis of electrospray-coated Tf680/TiO_2 nanoparticles and the Tf receptor had a binding affinity of K_D = 2.07 ± 1.06 nM, which is similar to the binding affinity of free Tf680 to the Tf receptor (K_D = 5.71 ± 3.15 nM) and was close to the reported binding affinity value for Tf to the Tf receptor (Figure 7, Table 2).[39,40] The slightly improved K_D for the electrospray-processed Tf680/TiO_2 nanoparticles compared to free Tf may be attributed to the multivalent effect due to multiple Tf680 molecules on a single nanoparticle. The conventionally prepared Tf680/TiO_2 nanoparticles showed worse binding with a significantly higher K_D value (21.86 ± 2.58 nM), possibly due to aggregation.

The *in vitro* cytotoxicity of conventional Tf/TiO_2, electrospray functionalized Tf/TiO_2, ^{18}FDG, and our CRIT treatment was assessed on MM1.S-Luc and HT1080 cells using an MTS assay. No obvious toxicity was observed from the cells treated with Tf/TiO_2 nanoparticles only, even at a concentration of 100 μg/mL, which indicates good cytocompatibility of both conventional and electrospray-functionalized nanoparticles. MM1.S cells treated with ^{18}FDG alone did not show obvious cytotoxicity at a dosage of 100 μCi/mL. Treatment of conventional Tf/TiO_2 nanoparticle internalized tumor cells with ^{18}FDG only decreased cell viability by 23%, while electrospray Tf/TiO_2 nanoparticles have up to 57% cell killing from CRIT treatment (Figure 8a). These results suggest that internalization of both nanoparticles and the radionuclide in cells is a prerequisite for CR-induced cytotoxicity. From these results, we hypothesize that the electrospray Tf/TiO_2

nanoparticles' larger surface area compared to the clustered conventional Tf/TiO_2 nanoparticles provides enhanced ROS generation under the Cerenkov radiation from radioisotopes which leads to more effective cancer cell killing. Similar results were obtained with the HT1080 cell line (Figure 8b).

Due to the success of electrospray functionalization of these nanomaterials, future work will focus on increasing production volume by microfabricating a multiplexed electrospray emitter array. This device will increase electrospray production rates by orders of magnitude and provide sufficient materials for testing in mouse cancer models and further develop this technique so it can be utilized for more applications.

CONCLUSIONS

Electrospray has provided a method for functionalizing metal oxide nanoparticles with proteins. The protein Tf was efficiently and controllably coated on the surface of TiO_2 nanoparticles. The coating thickness of Tf was tuned by adjusting the precursor concentration of Tf while keeping the TiO_2 number concentration constant. SMPS and TEM measurements closely matched the expected functionalized nanoparticle size for each Tf concentration. DLS hydrodynamic diameter measurement further validated the size data. Using MST, the functional properties and targeting activity of electrospray processed Tf proteins on the surface of TiO_2 nanoparticles were confirmed by measuring their binding efficiencies with Tf receptors, compared to a control. Results of *in vitro* studies showed that electrospray-coated Tf/TiO_2 nanoparticles improved cell killing for MM1.S multiple myeloma cells from 23% to 57% compared to Tf/TiO_2 nanoparticles prepared using conventional functionalization methods. Our results show that electrospray is an effective and highly controllable method of functionalizing nanoparticles with high monodispersity. In vivo assessment of this particle will focus on optimization of tumor uptake and Cerenkov light production of different radioisotopes to produce maximum CRIT effect.

METHODS

Materials.

Sucrose (BioXtra, ≥99.5%), ammonium acetate (anhydrous, for molecular biology, ≥99%), ammonium hydroxide, titanium(IV) isopropoxide (99.999% trace metals basis), nitric acid (≥99.999% trace metals basis), and transferrin (human, powder, BioReagent) were purchased from Sigma-Aldrich (Saint Louis, MO, USA). Fluorescent transferrin (Tf680, Alexa Fluor 680 Conjugate) was purchased from ThermoFisher Scientific (Waltham, MA, USA). The electron microscopy stain Nano-W was purchased from Nanoprobes Inc. (Upton, NY, USA). Ultrapure water (Milli-Q Advantage System, Millipore, USA) was used in all solutions and suspensions and had a resistivity of 18.3 MΩ-cm prior to the addition of chemicals and precursors.

TiO_2 Nanoparticle Synthesis.

Anatase-phase TiO_2 nanoparticles were synthesized by hydrolysis of titanium isopropoxide (TTIP) in an acidic ethanol/water solution which is heated in a hydrothermal Parr bomb (Parr Instrument Co., Moline, IL).[41] For synthesis of 25 nm diameter anatase TiO_2, the pH

of a 1:8 (v:v) ethanol/water solution was adjusted to 0.7 by adding nitric acid followed by dropwise addition of 1 mL of TTIP. After 4 h of stirring, the solution was added to the hydrothermal bomb and heated to 240 °C for 4 h without stirring. The particles were then cooled and washed with ethanol three times. For each wash, the nanoparticle batch was split between two 50 mL centrifuge tubes, and ethanol was added to fill the tubes. The samples were vortexed and sonicated before centrifugation at 10 000 rpm for 10 min. Supernatant was poured off, and then the particles were resuspended in ethanol. After washing, the nanoparticles were dried at 80 °C for preparation of stock TiO_2 suspensions.

Electrospray Processing.

A diagram of the electrospray system used in this work is shown in Figure 9. A 125 μm inner diameter (ID) capillary tube is supplied with the precursor suspension by a syringe pump (Harvard Apparatus, South Natick, MA). The distance from the tip of the capillary tube to the grounded collection solution is 10 cm. The collection solution consists of ultrapure water in a glass dish with nitric acid added to modify the conductivity to 0.3 S/m. A grounded electrode is added to the collection solution. A coaxial tube allows CO_2 to flow as a sheath around the capillary tube to suppress possible corona discharges.[42,43] The flow rate of the precursor suspension is controlled by the programmable syringe pump, while the flow rate of CO_2 is controlled by a mass flow controller (Omega Engineering, Inc., Stanford, CT). During electrospray processing the shape of the liquid meniscus jet at the end of the capillary is observed using a DALSA camera (CA-D6). A high voltage power supply (Bertan High Voltage, Hicksville, NY) was used at voltages between −5.5 and −6.5 keV to produce a stable Taylor Cone-jet in most experiments.

Nitric acid was used to modify the conductivity of the precursor suspension to 0.3 S/m but also to increase the zeta potential and stability of the precursor suspension. The concentration of TiO_2 nanoparticles in the precursor suspension was held constant at 1 mg/mL, and varying concentrations (0 to 25uM) of Tf were then added to control the final coating thickness after electrospray processing.

Tf/TiO_2 Nanoparticle Sizing and Stability.

The charged aerosolized Tf/TiO_2 nanoparticles were directly measured after their formation by a scanning mobility particle sizer (SMPS) system. Shown in Figure 9, the SMPS consists of a radioactive neutralizer, a nanodifferential mobility analyzer (DMA, TSI model 3071), and a condensation particle counter (CPC, TSI model 3025A). The nano DMA is used to measure particles from 3 to 80 nm. During measurement, the Tf/TiO_2 nanoparticles are first passed through the radioactive neutralizer which gives the particles a known charge distribution. The particles then pass through the DMA, where they are subjected to a radial electric field at atmospheric pressure. The Tf/TiO_2 nanoparticles move in the electric field, and only those with a specific mobility exit the DMA for a given electric field. Nanoparticles of each mobility are counted by the CPC as the electric field inside the DMA is varied stepwise. The number of Tf/TiO_2 nanoparticles measured for each mobility is then converted to a size distribution.

A solution of 0.1% (v/v) sucrose was used as a standard to determine droplet sizes for each electrospray operating condition. Sucrose was dissolved in deionized water and titrated with nitric acid until the electrical conductivity was measured at 0.3 S/m. Because the size of the produced droplets is primarily controlled by the electrical conductivity of the solution and the liquid flow rate, these parameters were carefully controlled and monitored. Droplet size was then calculated as described by Chen et al. for precursor flow rates between 0.3 and 1.5 μL/min, using the SMPS. Equation 1 is an empirical formula expressing that the primary droplet diameter D_d can be calculated for a known sucrose concentration C and sucrose particle diameter D_p.[42] These droplet size measurements were used to help determine the optimal concentrations of Tf and TiO_2 in the precursor suspension.

$$D_d = \frac{1}{C^{1/3}} D_p \quad (1)$$

Transmission electron microscopy (TEM, FEI Tecnai Spirit) was used to characterize the shape and size of the Tf/TiO_2 nanoparticles. TEM images were analyzed using ImageJ software (Rasband, W.S., ImageJ, U.S. National Institutes of Health, Bethesda, Maryland, USA). Samples were collected on a 300-mesh copper TEM grid placed on a grounded surface below the emitter. Nano-W was used to stain the Tf on the TiO_2 nanoparticle surface and make it electron dense enough to have contrast in TEM images.

X-ray powder diffraction (XRD) was used to confirm the crystal phase of TiO_2 and was carried out using a Bruker D8 Advance (Bruker AXS, Germany).

Dynamic light scattering (ZetaSizer Nano ZS, Malvern Instruments Inc.) was used to measure the hydrodynamic diameter of Tf/TiO_2 nanoparticles and zeta potential of precursor suspensions. All measurements were made at 25 °C with 173° back-angle scattering. For zeta potential measurements, the pH was adjusted with nitric acid and ammonium hydroxide to determine the isoelectric point.

Tf/TiO_2 Binding Affinity.

Microscale thermophoresis (MST) was used to determine the binding affinities between Tf680/TiO_2 nanoparticles prepared using the conventional method described in Kotagiri et al.,[3] Tf680/TiO_2 nanoparticles prepared via electrospray (1:3, Tf:TiO_2, wt:wt), free Tf680, and the Tf receptor. Analyses were performed on a Monolith NT115.pico instrument (Nano Temper Technologies GmbH, Munich, Germany) using Nanotemper glass capillaries with an MST power of 40% and a red channel LED power of 10%. For MST measurements, Tf680 was used at a constant concentration of 5 nM. Transferrin receptors were diluted 16 times in a 1:1 serial dilution from 0.5 mM to a final concentration of 15.25 nM and incubated at room temperature with the test particles for at least 5 min before measurement. Data analysis was performed with Monolith Affinity analysis software (Nano Temper Technologies, Munich, Germany).

Cancer Cell Culture.

All cell lines underwent Short Tandem Repeat (STR) profiling and testing for mycoplasma contamination. MM1.S-Luc cells were cultured in RPMI1640 medium containing 10% heat-inactivated fetal bovine serum (FBS) and 2-mercaptoethanol (50 μM final) and 1× of all of the following: penicillin/streptomycin (100 μg mL^{-1} final), sodium pyruvate (1 mM final), nonessential amino acids, HEPES (10 mM final), and L-glutamine. HT1080 cells were cultured in Dulbecco's Modified Eagle's Medium containing 10% FBS, L-glutamine (2 mM), penicillin (100 units/mL), and streptomycin (100 μg/mL), incubated at 37 °C in a humidified atmosphere of 5% CO_2 and 95% air.

In Vitro Cell Viability Assays: Understanding the CRIT Efficiency of Tf/TiO_2.

The MTS (3-(4,5-dimethylthiazol-2-yl)-5-(3-carboxymethoxyphenyl)-2-(4-sulfophenyl)-2*H*-tetrazolium) assay, a calorimetric assay for assessing viability of cell culture, was performed using the CellTiter 96 Aqueous Non-Radioactive Cell Proliferation Assay kit (Promega Co., Fitchburg, WI, USA). Cells (5×10^5 for MM1.S and 5×10^4 for HT1080) were treated with 100 μg/mL of Tf-coated nanoparticles in a 24-well plate for 16 h based on the CRIT experiments from previous studies.[3] After removing the culture media, cells were washed twice with PBS to remove any noninternalized nanoparticles before introducing 100 μCi/mL of ^{18}FDG for CRIT treatment. The cells were incubated another 48 h before MTS assays were performed. Absorbance measurements were taken on a Biotek Synergy HTX multimode platereader.

ACKNOWLEDGMENTS

Support was provided by NIH-NCI U54CA199092 and NIH-NIBIB R01EB021048. This work was performed in part at the Nano Research Facility (NRF) of Washington University in St. Louis. We would like to thank Jim Ballard at the McKelvey School of Engineering at Washington University in St. Louis Engineering Communication Center for his help reviewing and editing this paper.

REFERENCES

(1). Edwards BK; Ward E; Kohler BA; Eheman C; Zauber AG ; Anderson RN; Jemal A; Schymura MJ; Lansdorp-Vogelaar I; Seeff LC; et al. Annual Report to the Nation on the Status of Cancer, 1975–2006, Featuring Colorectal Trends and Impact of Interventions (Risk Factors, Screening, and Treatment) to Reduce Future Rates. Cancer 2010, 116 (3), 544–573. [PubMed: 19998273]

(2). Bhattacharya R; Patra CR; Verma R; Kumar S; Greipp PR; Mukherjee P Gold Nanoparticles Inhibit the Proliferation of Multiple Myeloma Cells. Adv. Mater 2007, 19 (5), 711–716.

(3). Kotagiri N; Sudlow GP; Akers WJ; Achilefu S Breaking the Depth Dependency of Phototherapy with Cerenkov Radiation and Low Radiance Responsive Nanophotosensitizers. Nat. Nanotechnol 2015, 10 (4), 370. [PubMed: 25751304]

(4). Soodgupta D; Pan D; Cui G; Senpan A; Yang X; Lu L; Weilbaecher KN; Prochownik EV; Lanza GM; Tomasson MH Small Molecule MYC Inhibitor Conjugated to Integrin-Targeted Nanoparticles Extends Survival in a Mouse Model of Disseminated Multiple Myeloma. Mol. Cancer Ther 2015, 14 (6), 1286–1294. [PubMed: 25824336]

(5). Orlowski RZ; Nagler A; Sonneveld P; Bladé J; Hajek R; Spencer A; San Miguel J; Robak T; Dmoszynska A; Horvath N; et al. Randomized Phase III Study of Pegylated Liposomal Doxorubicin Plus Bortezomib Compared With Bortezomib Alone in Relapsed or Refractory Multiple Myeloma: Combination Therapy Improves Time to Progression. J. Clin. Oncol 2007, 25 (25), 3892–3901. [PubMed: 17679727]

(6). Wu Y; Li L; Mao Y; Lee LJ Static Micromixer–Coaxial Electrospray Synthesis of Theranostic Lipoplexes. ACS Nano 2012, 6 (3), 2245–2252. [PubMed: 22320282]

(7). Lin J; Wang S; Huang P; Wang Z; Chen S; Niu G; Li W; He J; Cui D; Lu G Photosensitizer-Loaded Gold Vesicles with Strong Plasmonic Coupling Effect for Imaging-Guided Photothermal/Photodynamic Therapy. ACS Nano 2013, 7 (6), 5320–5329. [PubMed: 23721576]

(8). Cui S; Yin D; Chen Y; Di Y; Chen H; Ma Y; Achilefu S; Gu Y I*n Vivo* Targeted Deep-Tissue Photodynamic Therapy Based on Near-Infrared Light Triggered Upconversion Nanoconstruct. ACS Nano 2013, 7 (1), 676–688. [PubMed: 23252747]

(9). Wang J; Zhu G; You M; Song E; Shukoor MI; Zhang K; Altman MB; Chen Y; Zhu Z; Huang CZ Assembly of Aptamer Switch Probes and Photosensitizer on Gold Nanorods for Targeted Photothermal and Photodynamic Cancer Therapy. ACS Nano 2012, 6 (6), 5070–5077. [PubMed: 22631052]

(10). Meng H; Liong M; Xia T; Li Z; Ji Z; Zink JI; Nel AE Engineered Design of Mesoporous Silica Nanoparticles to Deliver Doxorubicin and P-Glycoprotein siRNA to Overcome Drug Resistance in a Cancer Cell Line. ACS Nano 2010, 4 (8), 4539–4550. [PubMed: 20731437]

(11). Hogan CJ Jr; Carroll JA; Rohrs HW; Biswas P; Gross ML Combined Charged Residue-Field Emission Model of Macromolecular Electrospray Ionization. Anal. Chem. 2009, 81 (1), 369–377. [PubMed: 19117463]

(12). Shah VB; Biswas P Aerosolized Droplet Mediated Self-Assembly of Photosynthetic Pigment Analogues and Deposition onto Substrates. ACS Nano 2014, 8 (2), 1429–1438. [PubMed: 24422474]

(13). Hogan CJ Jr.; Biswas P Narrow Size Distribution Nanoparticle Production by Electrospray Processing of Ferritin. J. Aerosol Sci 2008, 39 (5), 432–440.

(14). Kavadiya S; Niedzwiedzki DM; Huang S; Biswas P Electrospray-Assisted Fabrication of Moisture-Resistant and Highly Stable Perovskite Solar Cells at Ambient Conditions. Adv. Energy Mater 2017, 7 (18), 1700210.

(15). Raliya R; Saha D; Chadha TS; Raman B; Biswas P Non-Invasive Aerosol Delivery and Transport of Gold Nanoparticles to the Brain. Sci. Rep 2017, 7, 44718. [PubMed: 28300204]

(16). Lohcharoenkal W; Wang L; Chen YC; Rojanasakul Y Protein Nanoparticles as Drug Delivery Carriers for Cancer Therapy. BioMed Res. Int 2014, 2014, 1.

(17). Qu J; Liu Y; Yu Y; Li J; Luo J; Li M Silk Fibroin Nanoparticles Prepared by Electrospray as Controlled Release Carriers of Cisplatin. Mater. Sci. Eng. C 2014, 44, 166–174.

(18). Wu Y; MacKay JA; McDaniel JR; Chilkoti A; Clark RL Fabrication of Elastin-Like Polypeptide Nanoparticles for Drug Delivery by Electrospraying. Biomacromolecules 2009, 10 (1), 19–24. [PubMed: 19072041]

(19). Yaghoobi N; Majidi RF; Faramarzi M; Baharifar H; Amani A Preparation, Optimization and Activity Evaluation of PLGA/Streptokinase Nanoparticles Using Electrospray. Adv. Pharm. Bull 2017, 7 (1), 131. [PubMed: 28507947]

(20). Gulfam M; Kim J.-e.; Lee JM; Ku B; Chung BH; Chung BG Anticancer Drug-Loaded Gliadin Nanoparticles Induce Apoptosis in Breast Cancer Cells. Langmuir 2012, 28 (21), 8216–8223. [PubMed: 22568862]

(21). Raliya R; Singh Chadha T; Haddad K; Biswas P Perspective on Nanoparticle Technology for Biomedical Use. Curr. Pharm. Des 2016, 22 (17), 2481–2490. [PubMed: 26951098]

(22). Kavadiya S; Biswas P Design of Cerenkov-assisted Photo-activation of TiO_2 Nanoparticles and Reactive Oxygen Species Generation for Cancer Treatment. J. Nucl. Med 2018, 215608.

(23). Daniels TR; Delgado T; Rodriguez JA; Helguera G; Penichet ML The Transferrin Receptor Part I: Biology and Targeting with Cytotoxic Antibodies for the Treatment of Cancer. Clin. Immunol 2006, 121 (2), 144–158. [PubMed: 16904380]

(24). Daniels TR; Delgado T; Helguera G; Penichet ML The Transferrin Receptor Part II: Targeted Delivery of Therapeutic Agents into Cancer Cells. Clin. Immunol 2006, 121 (2), 159–176. [PubMed: 16920030]

(25). Akpan U; Hameed B Parameters Affecting the Photocatalytic Degradation of Dyes Using TiO_2-Based Photocatalysts: A Review. J. Hazard. Mater 2009, 170 (2–3), 520–529. [PubMed: 19505759]

(26). Foster HA; Ditta IB; Varghese S; Steele A Photocatalytic Disinfection using Titanium Dioxide: Spectrum and Mechanism of Antimicrobial Activity. Appl. Microbiol. Biotechnol 2011, 90 (6), 1847–1868. [PubMed: 21523480]

(27). Maness P-C; Smolinski S; Blake DM; Huang Z; Wolfrum EJ; Jacoby WA Bactericidal Activity of Photocatalytic TiO_2 Reaction: toward an Understanding of Its Killing Mechanism. Appl. Environ. Microbiol 1999, 65 (9), 4094–4098. [PubMed: 10473421]

(28). Pelaez M; Nolan NT; Pillai SC; Seery MK; Falaras P; Kontos AG; Dunlop PS; Hamilton JW; Byrne JA; O'shea K; et al. A Review on the Visible Light Active Titanium Dioxide Photocatalysts for Environmental Applications. Appl. Catal., B 2012, 125, 331–349.

(29). Jiang J; Oberdörster G; Elder A; Gelein R; Mercer P; Biswas P Does Nanoparticle Activity Depend upon Size and Crystal Phase? Nanotoxicology 2008, 2 (1), 33–42. [PubMed: 20827377]

(30). Greenstein S; Krett NL; Kurosawa Y; Ma C; Chauhan D; Hideshima T; Anderson KC; Rosen ST Characterization of the MM. 1 Human Multiple Myeloma (MM) Cell Lines. Exp. Hematol 2003, 31 (4), 271–282. [PubMed: 12691914]

(31). Cho K; Hogan CJ; Biswas P Study of the Mobility, Surface Area, and Sintering Behavior of Agglomerates in the Transition Regime by Tandem Differential Mobility Analysis. J. Nanopart. Res 2007, 9 (6), 1003–1012.

(32). Cheng Y-S; Allen MD; Gallegos DP; Yeh H-C; Peterson K Drag Force and Slip Correction of Aggregate Aerosols. Aerosol Sci. Technol 1988, 8 (3), 199–214.

(33). Kilar F; Simon I The Effect of Iron Binding on the Conformation of Transferrin. A Small Angle X-ray Scattering Study. Biophys. J 1985, 48 (5), 799–802. [PubMed: 4074838]

(34). Wienken CJ; Baaske P; Rothbauer U; Braun D; Duhr S Protein - Binding Assays in Biological Liquids Using Microscale Thermophoresis. Nat. Commun 2010, 1, 100. [PubMed: 20981028]

(35). Seidel SA; Dijkman PM; Lea WA; van den Bogaart G; Jerabek-Willemsen M; Lazic A; Joseph JS; Srinivasan P; Baaske P; Simeonov A; et al. Microscale Thermophoresis Quantifies Biomolecular Interactions Under Previously Challenging Conditions. Methods 2013, 59 (3), 301–315. [PubMed: 23270813]

(36). Garcia-Bonete M-J; Jensen M; Recktenwald CV; Rocha S; Stadler V; Bokarewa M; Katona G Bayesian Analysis of MicroScale Thermophoresis Data to Quantify Affinity of Protein: Protein Interactions with Human Survivin. Sci. Rep 2017, 7 (1), 16816. [PubMed: 29196723]

(37). Jerabek-Willemsen M; Wienken CJ; Braun D; Baaske P; Duhr S Molecular Interaction Studies Using Microscale Thermophoresis. Assay Drug Dev. Technol 2011, 9 (4), 342–353. [PubMed: 21812660]

(38). Lippok S; Seidel SA; Duhr S; Uhland K; Holthoff H-P; Jenne D; Braun D Direct Detection of Antibody Concentration and Affinity in Human Serum Using Microscale Thermophoresis. Anal. Chem 2012, 84 (8), 3523–3530. [PubMed: 22397688]

(39). Kleven MD; Jue S; Enns CA Transferrin Receptors TfR1 and TfR2 Bind Transferrin through Differing Mechanisms. Biochemistry 2018, 57 (9), 1552–1559. [PubMed: 29388418]

(40). Zhang D; Lee HF; Pettit SC; Zaro JL; Huang N; Shen WC Characterization of Transferrin Receptor-Mediated Endocytosis and Cellular Iron Delivery of Recombinant Human Serum Transferrin from Rice (Oryza Sativa L.). BMC Biotechnol. 2012, 12, 92. [PubMed: 23194296]

(41). Chae SY; Park MK; Lee SK; Kim TY; Kim SK; Lee WI Preparation of Size-Controlled TiO_2 Nanoparticles and Derivation of Optically Transparent Photocatalytic Films. Chem. Mater 2003, 15 (17), 3326–3331.

(42). Chen D-R; Pui DY; Kaufman SL Electrospraying of Conducting Liquids for Monodisperse Aerosol Generation in the 4 nm to 1.8 μm Diameter Range. J. Aerosol Sci 1995, 26 (6), 963–977.

(43). De Juan L; de la Mora JF On-line Sizing of Colloidal Nanoparticles via Electrospray and Aerosol Techniques; ACS Publications: 1996.

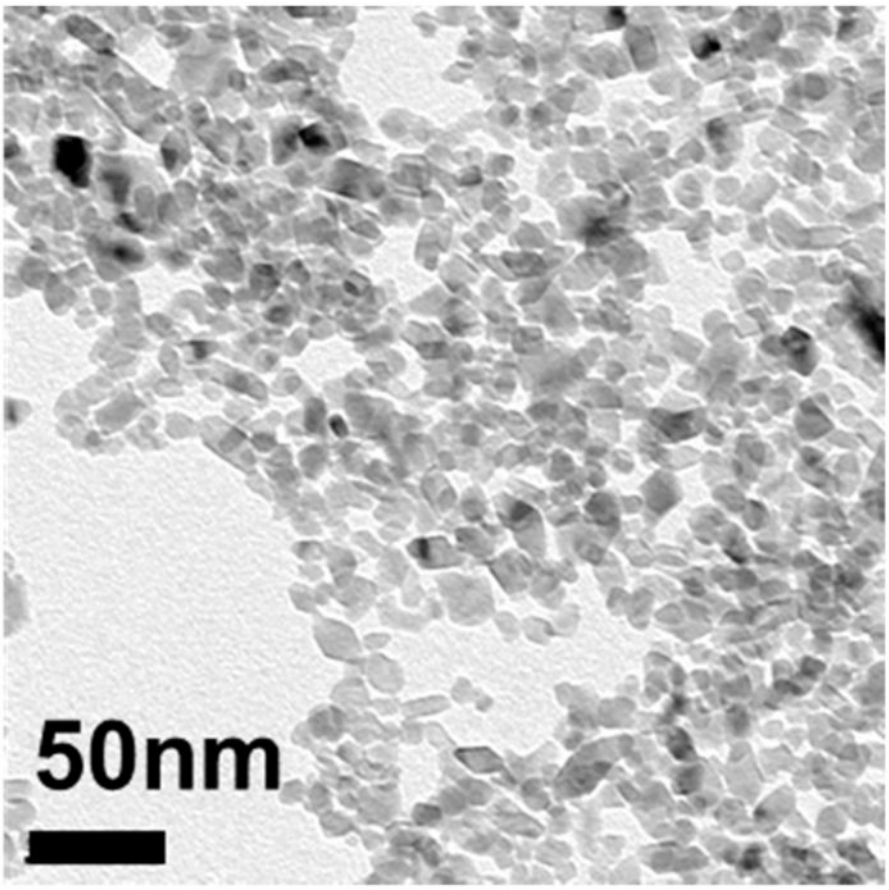

Figure 1.
TEM of 25 nm TiO_2 nanoparticles after synthesis.

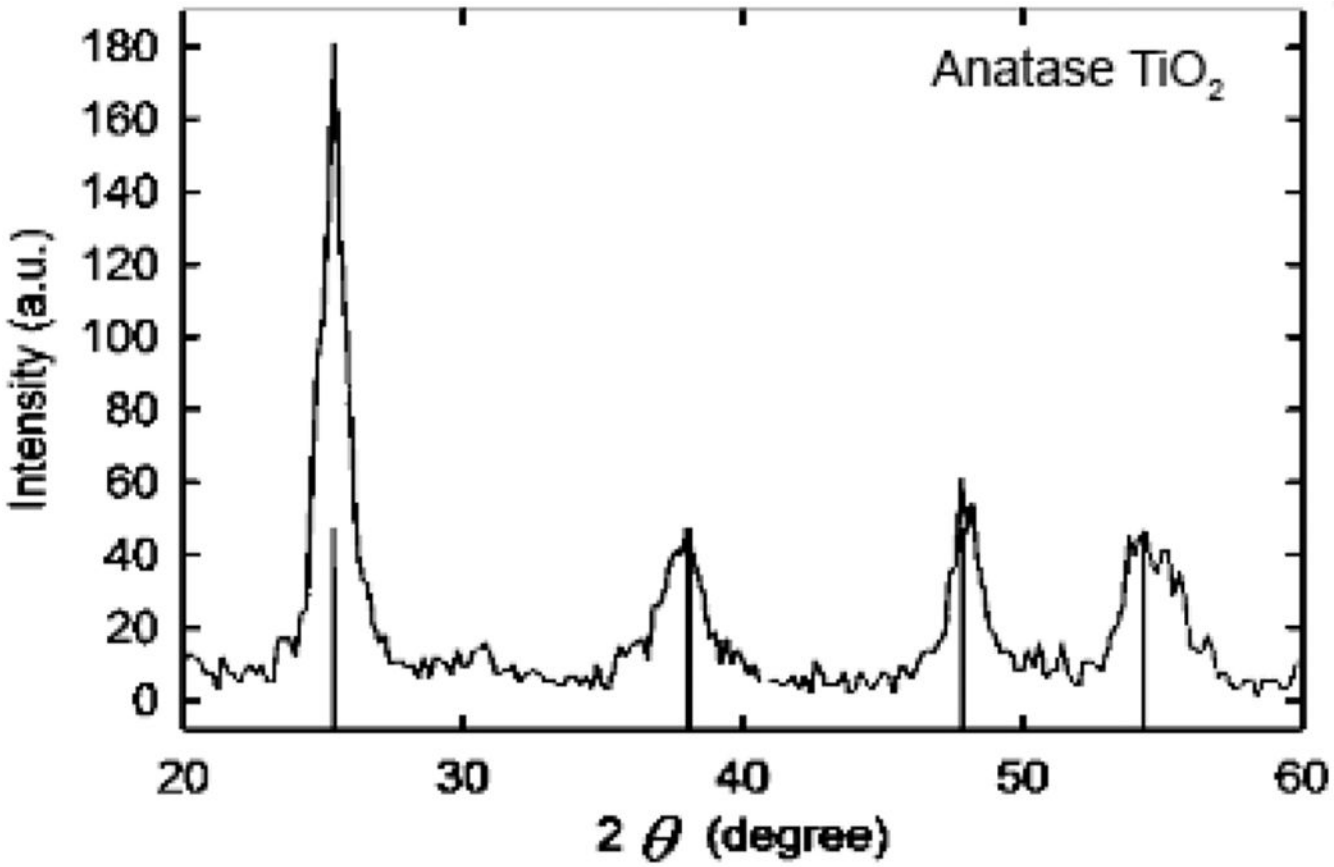

Figure 2.
XRD of nanoparticles indicating anatase TiO_2.

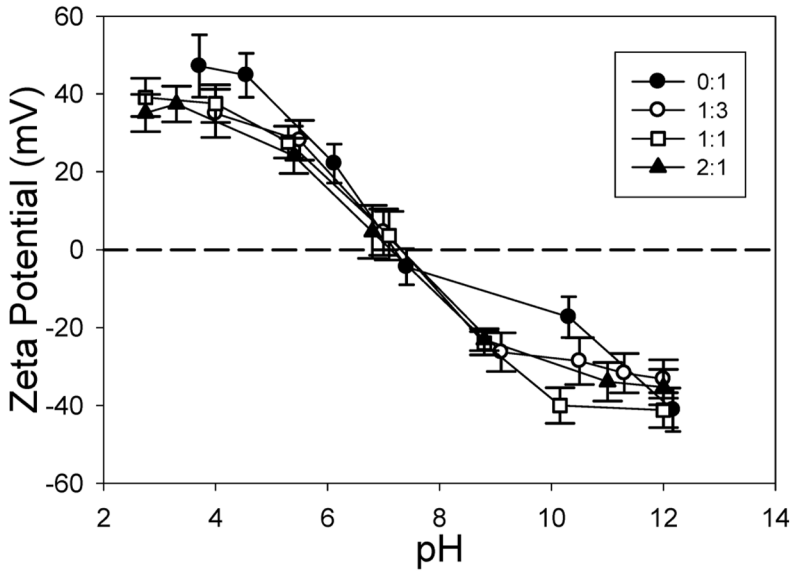

Figure 3.

Isoelectric point measurements of electrospray precursor solutions with varying concentrations of Tf to TiO_2. Ratio of Tf:TiO_2 (wt:wt) ranged from 0:1 to 2:1.

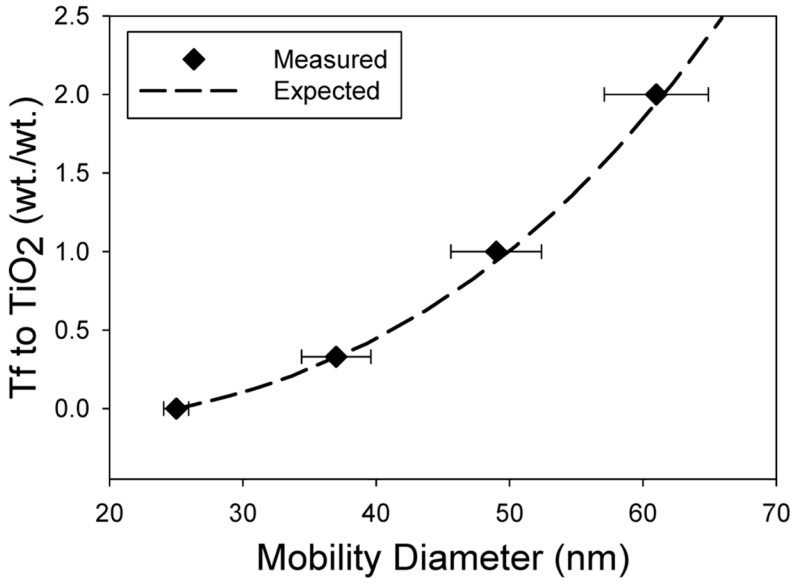

Figure 4.
SMPS measured geometric mean mobility diameter for varying Tf to TiO_2 ratios.

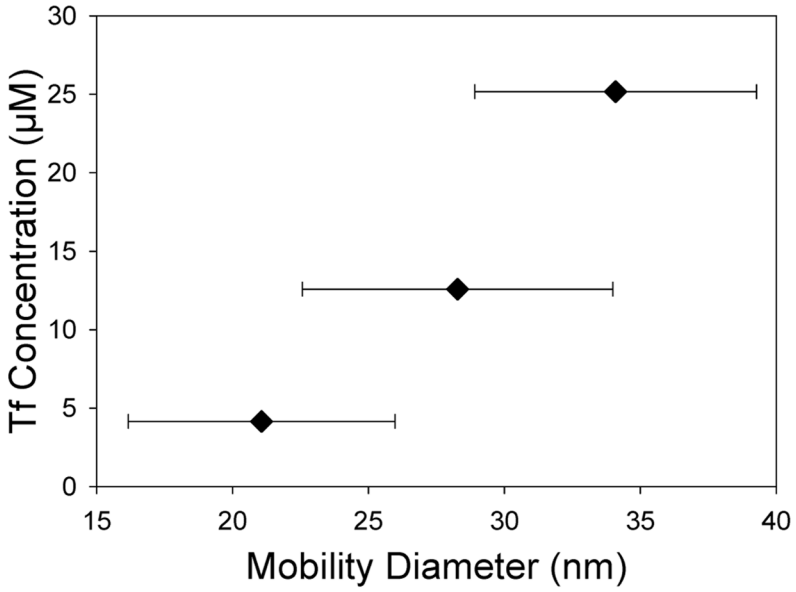

Figure 5.
SMPS measured geometric mean mobility diameter for varying Tf nanoparticle sizes.

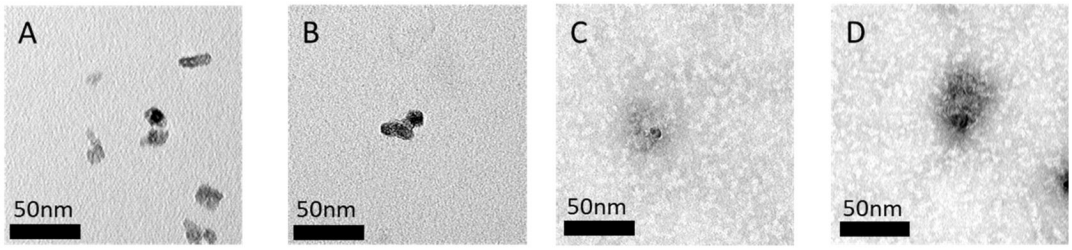

Figure 6.

Transmission electron microscopy images of TiO_2 nanoparticles that have been electrospray coated with varying concentrations of Tf. Ratio of Tf:TiO_2 is wt:wt: (A) 0:1, (B) 1:3, (C) 1:1, and (D) 2:1.

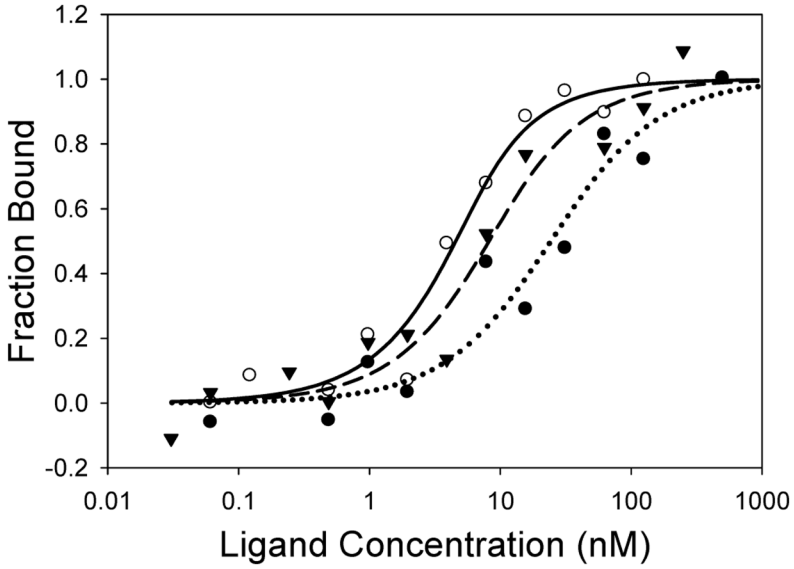

Figure 7.

Binding affinity of electrospray-coated Tf680/TiO_2 nanoparticle (open circle, K_D = 2.07 nm), conventionally prepared Tf680/TiO_2 nanoparticle (solid circle, K_D = 21.86 nm), and free Tf680 (triangle, K_D = 5.71 nm) with transferrin receptor analyzed by microscale thermophoresis.

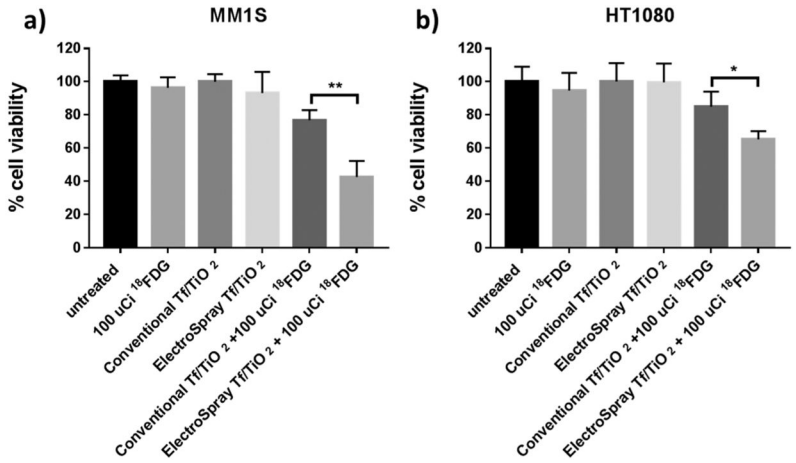

Figure 8.

Cell viability assay comparing the conventional Tf/TiO_2 and electrospray Tf/TiO_2 constructs with and without exposure to 100 uCi ^{18}FDG on (a) MM1S cells and (b) HT1080 cells.

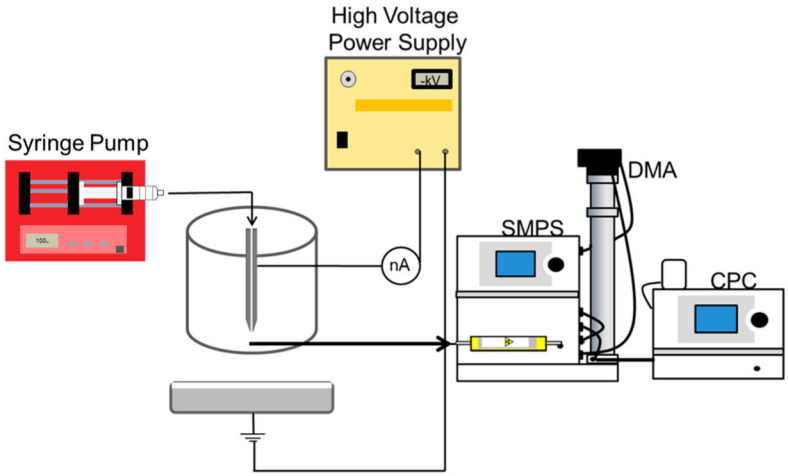

Figure 9.

Electrospray setup with SMPS particle sampling for size measurements. A syringe pump supplies the precursor suspension to the electrospray capillary with a grounded capture solution below. A high voltage power supply controls the electric field. A scanning mobility particle sizer (SMPS) measures the mobility size of the electrospray-coated particles by first neutralizing the particles and passing them through a differential mobility analyzer and then counting them using a condensation particle counter.

Table 1.

DLS Number Mean Diameter and Polydispersity Index (PDI) for TiO_2 and Tf/TiO_2 Nanoparticles Synthesized with Varying Concentrations of Tf[a]

material	number mean diameter (nm)	zeta potential (mV)	PDI
bare TiO_2	25.38	45.1 ± 10.8	0.38
Tf:TiO_2 1:3	37.74	35 ± 12.4	0.293
Tf:TiO_2 1:1	47.39	37.5 ± 9.68	0.331
Tf:TiO_2 2:1	58.54	37.4 ± 9.2	0.394

[a]All measurements were taken at pH 4.

Table 2.

MST Binding Data for the Fluorescence Protein Coated TiO_2 Nanoparticles with the Transferrin Receptor[a]

compound	K_D (nM) (Mean ± SD)	goodness of fit (R^2)
Tf680/TiO_2 conventional	21.86 ± 2.58	0.7134
Tf680/TiO_2 electrospray	2.07 ± 1.06	0.8540
free Tf680	5.71 ± 3.15	0.7440

[a]Tf680/TiO_2 conventional was prepared as described by Kotagiri et al.[3]